Food Hydrocolloids for Health 1 (2021) 100041

Contents lists available at ScienceDirect

Food Hydrocolloids for Health

journal homepage: www.elsevier.com/locate/fhfh

Microfluidics-based encapsulation of isoniazid in egg white/carrageenan microparticles for sustained release

Robinson C. Marengo[a,b], Luciano N. Mengatto[a], María L. Olivares[a], Claudio L.A. Berli[a,*]

[a] INTEC (Universidad Nacional del Litoral-CONICET), Predio CCT-CONICET Santa Fe, RN 168, Santa Fe 3000, Argentina
[b] Centro Universitario Gálvez (Universidad Nacional del Litoral), Florentino Ameghino 50, Gálvez, Santa Fe, Argentina

ARTICLE INFO

Keywords:
Isoniazid
Encapsulation
Microfluidics
Egg white/carrageenan
Drug release

ABSTRACT

The prevalence of tuberculosis continuously grows and there is an imperious need to improve the therapeutic efficacy of approved drugs for clinical use. Here we report the encapsulation of isoniazid (INH) in egg white/κ-carrageenan microparticles, which are intended for drug vehiculation through the gastrointestinal tract and controlled release in the ileum. Spherical and highly monodisperse microparticles (255 mm average diameter) were obtained by droplet-based microfluidics and subsequent microwave irradiation. The entire amount of INH added to the particles was encapsulated. Infrared spectra revealed the formation of esters, hydrogen bonding, and Maillard reaction in the biopolymer matrix. *In vitro* release experiments were carried out in media that systematically emulate the stomach and intestinal tract conditions: 37 °C, NaCl 0.05 mol/L, pH 1.6, for the first 2 h, and Tris–HCl 0.1 mol/L, pH 7, for the next 24 h. A small fraction of the loaded INH was released in the first medium and most of the drug was progressively delivered in the second medium. The release profiles of microparticles were analyzed by using classical kinetic models, which enabled to hypothesize the release mechanism of INH from the biopolymer matrix. This knowledge, together with the ability to control the governing parameters of microfluidic elaboration, opens further possibilities for designing optimal prototypes for sustained release.

1. Introduction

Tuberculosis (TB) is a millenary disease that increasingly challenges public health systems (Barberis, Bragazzi, Galluzzo & Martini, 2017). In the last decades, AIDS, smoke, and the inefficacy of BCG vaccine have risen TB prevalence. On the other hand, long-term treatments with drugs causing strong side effects may induce therapy interruptions, which has negative consequences beyond the patient health, notably the risk of appearance of multidrug resistant bacteria. Therefore, decreasing the drug concentration and the number of doses is highly desirable. Regarding the pharmaceutical formulation, the main challenges are improving the encapsulation for controlled drug delivery and enhancing the stability of the active molecules.

The last aspect is particularly important for the simultaneous use of two anti-TB drugs, such as rifampicin (RIF) and isoniazid (INH). In acidic medium, RIF hydrolyzes to 3-formyl rifamycin SV (3FRSV) and this reaction is accelerated in the presence of INH, because this drug interacts with 3FRSV producing isonicotinyl hydrazone. Both RIF derivatives present low solubility and absorption in the gastrointestinal tract, which affect their anti-TB efficacy (Singh, Mariappan, Sankar, Sarda & Singh, 2001). Therefore, in the formulation of the two-drug fixed dose combination, RIF and INH must be compartmentalized to preserve RIF stability. Compartments can include micro-nanoparticles, micelles, hydrogels, or 3D printed systems (Ghanizadeh Tabriz et al., 2021; Singh, Bhandari & Kaur, 2013). For example, if only one of the drugs is encapsulated, the non-encapsulated drug can be absorbed in the stomach and the other one can be released later on in the ileum. As INH is protonated in acidic media (pK_a 2), the drug hardly permeates through the stomach mucosa and can be later absorbed by the small intestine (Mwila & Walker, 2020). Thus, a promising strategy is encapsulating INH in a system that retains the drug in the stomach and delivers only in the ileum, so that RIF could be released in the stomach in the absence of INH. In fact, it has been recently demonstrated that INH-loaded gastric-resistant microspheres of hydroxypropyl methylcellulose acetate succinate and Eudragit® L100 polymers decreased the degradation of RIF (Mwila & Walker, 2020).

In addition to microparticles intended for oral administration, which are normally produced by emulsification and solvent evaporation methods (Grenha et al., 2020; Mwila & Walker, 2020), smaller microparticles produced by the spray-drying technique can be used as inhalable drug carriers (Pandey, Yadav & Mishra, 2015; Rodrigues et al., 2020). Actually, microparticulate formulations are producing a strong therapeutic impact in medical technology, and nowadays they are globally demanded due the great advantages that offer the implementation of controlled drug release (Bale, Khurana, Reddy, Singh & Godugu, 2016).

* Corresponding author.
E-mail address: cberli@santafe-conicet.gov.ar (C.L.A. Berli).

https://doi.org/10.1016/j.fhfh.2021.100041
Received 24 July 2021; Received in revised form 9 October 2021; Accepted 15 November 2021

Here it is worth noting that, apart from microparticulate formulations, other approaches to encapsulate INH are currently under study, such as micelles (Rani et al., 2018; Sheth, Tiwari & Bahadur, 2018), liposomes (Gürsoy, Kut & Özkırımlı, 2004; Nkanga, Krause, Noundou & Walker, 2017), and nanoparticle (Booysen et al., 2013; Mukhtar et al., 2020; Shrimal, Jadeja & Patel, 2020) systems. In this context, here we explore the encapsulation of INH in a microparticulate system aimed to attain: (*i*) high levels of drug loading in hydrophilic biopolymers, (*ii*) sustained release in hydrophilic medium avoiding burst release, and (*iii*) preferential INH delivery in the ileum, preventing RIF degradation in the stomach.

Most of the reported works on microparticle encapsulation of INH, as those mentioned above (Grenha et al., 2020; Mwila & Walker, 2020; Pandey et al., 2015; Rodrigues et al., 2020), employ conventional high-energy methods. Among the modern low-energy methods, droplet-based microfluidics has become a recognized technology for producing functional microparticles (Kong et al., 2012; Wu et al., 2013). Briefly, droplets of a polymer solution are generated in oil phase and then converted into microparticles by using chemical and/or physical curing methods. Concerning TB drugs, the approach has been successfully used to encapsulate RIF in core-shell microspheres made from poly(lactic-co-glycolic acid) and alginate (Choi, Seo, Kim, Kim & Kim, 2017; Kim et al., 2014). In a previous work (Marengo, Olivares & Berli, 2019), we have reported a microfluidic-based process for the production of protein/polysaccharide microparticles, which were able to encapsulate 100% of a model hydrophilic active, retaining the active in oil medium for several months, and gradually delivering the active in aqueous medium. In the present work, we take advantage of the versatility of both the microfluidic platform and the biopolymer matrix to investigate the encapsulation and release of INH. We used microwave (MW) irradiation as curing method to avoid the addition of chemical agents. The molecular interactions inside the biopolymer matrix were studied by infrared (IR) spectroscopy. Besides, the kinetics of INH delivery was analyzed in the framework of classical release models.

2. Materials and methods

2.1. Materials

Transparent PMMA sheets were acquired from a local market (Acrimev, Santa Fe, Argentina). Ethanol 99% (Cicarelli, San Lorenzo, Argentina) was used in PMMA bonding. Push-in fittings with M5 thread and OD 4 mm tubing (Festo, Martinez, Argentina) were used as connectors at the chip inlet/outlets. Food grade olive oil (Olivi Hnos., Mendoza, Argentina) with viscosity equal to 81 mPas was used as the continuous oil phase. Fresh chicken eggs (no more than two days after production) were purchased from a local market. The same market was used during the experimental program, with the purposes of maintaining the hen species and breeding conditions. Besides, the pH of the extracted egg withe was monitored for quality control. Carrageenan (CG) Type I, 80% kappa and 20% lambda, was obtained from Sigma Chemicals (Sigma-Aldrich, St. Louis, USA). INH, isoniazid analytical standard, was purchased from Sigma-Aldrich (India). Potassium bromide for infrared spectroscopy was acquired from Sigma-Aldrich (Steinheim, Germany). Water was ultrapure (Millipore, USA). Methanol (J.T. Baker, Trinidad and Tobago) and acetonitrile (J.T. Baker, China) were HPLC grade. Potassium phosphate monobasic (KH_2PO_4), sodium chloride (NaCl) and hydrochloric acid (HCl) were acquired from Cicarelli (San Lorenzo, Argentina), and hydroxymethyl aninomethane (Tris) from Biopack (Buenos Aires, Argentina).

2.2. Microfluidic chip fabrication

Microfluidic device was fabricated as previously reported (Marengo et al., 2019) by using CO_2 laser PLS Platform (Universal Laser System, Scottsdale, USA). The chips were fabricated from two PMMA layers that were micromachined by laser ablation. The top layer contained the inlet and outlet ports. The bottom layer contained the microchannels, which have trapezoidal cross-sections, as typically produced by laser engraving (Hong et al., 2010; Liu et al., 2017). Average cross-sectional microchannel width was about 360 μm throughout the fluidic circuit. The PMMA layers were bonded by using a solvent assisted technique that employs ethanol, mild pressure, and 10 min at 75 °C (Bamshad, Nikfarjam & Khaleghi, 2016; Liga, Morton & Kersaudy-Kerhoas, 2016). Fig. 1a shows an example of the resulting chips, displaying the fluidic network with a cross-shaped junction and a short serpentine. Push-in fittings with M5 thread were adjusted in the inlet/oulet ports (not shown in Fig. 1a). The inlets were connected to syringe pumps (Model PC11UBT, Apema, Villa Domínico, Argentina) by using OD 4 mm teflon tubing; the outlet was connected to sample collecting reservoirs.

2.3. Sample preparation

Chicken eggs were hand-broken and egg white (EW) was carefully separated without contamination. The EW was filtered with a gauze and then gently stirred to provide homogeneous mixture. The pH of the EW solution was 9, as measured with a pH-meter (Hanna Instruments S.L., Eibar, Spain). It is worth noting that EW solution is the original egg white, without added water. A 0.15% (w/v) CG solution was prepared. The dry powder was sprinkled on purified water at room temperature and then subjected to magnetic stirring for 40 min. Subsequently, 30 mg of INH was dissolved in the CG solution. Complete dissolution of the drug was observed at this step. Then EW and CG solutions were mixed at 1:1 ratio by magnetic stirring for 40 min. The concentration of INH was 0.4% w/v in the CG solution and 0.2% w/v in the final mixture (EW/CG 1:1). The final solution was set at pH 9.3 to assure the co-solubility of the biopolymers (Marengo et al., 2019). The stability of INH at this pH was checked by HPLC quantification and chromatograms inspection (see below Section 2.8); no alterations of the drug were observed.

2.4. Microparticles generation

The injection of reagents was carried out at controlled flow rates by using syringe pumps. The aqueous phase (EW/CG mixture and INH) was injected in the middle channel of the cross-junction and the organic phase (oil) in the transverse channels (Fig. 1a). The flow rates of the aqueous (EW/CG/INH mixture) and the oil phases were set to 0.5 mL/h and 3.5 mL/h, respectively. The device was allowed to reach a steady regime before collecting the microdroplets. The process was imaged by using a USB microscope mounted on the chip platform; typical captures of droplet generation are illustrated in Fig. 1b and c.

2.5. Microparticles curing

Droplets collected in glass tubes were subjected to microwave (MW) irradiation in a laboratory oven (BGH, Model B330DSS, Río Grande, Argentina) to obtain microparticles resistant to dilution, shearing, and further manipulation. Further, to explore different microstructures and release profiles, two MW conditions were evaluated: 270 W and 900 W for 15 s. After the treatment, solid microparticles suspended in the oil-phase were obtained. The microparticles sediment at rest in the oil phase, however they were highly stable against flocculation, even after 30 days of storage. Since all the aqueous phase (EW/CG/INH mixture) injected to the chip finally formed microparticles, and INH solubility in oil is very low (logP = −0.64) (Handbook, 2008), the encapsulation efficiency was considered to be 100%. Furthermore, the high INH hydrophilicity ensures that leakage to the oil phase (during microparticles generation, manipulation, or storage) is negligible, meaning that INH molecules are retained into the microparticles and are delivered upon contact with the release buffers only.

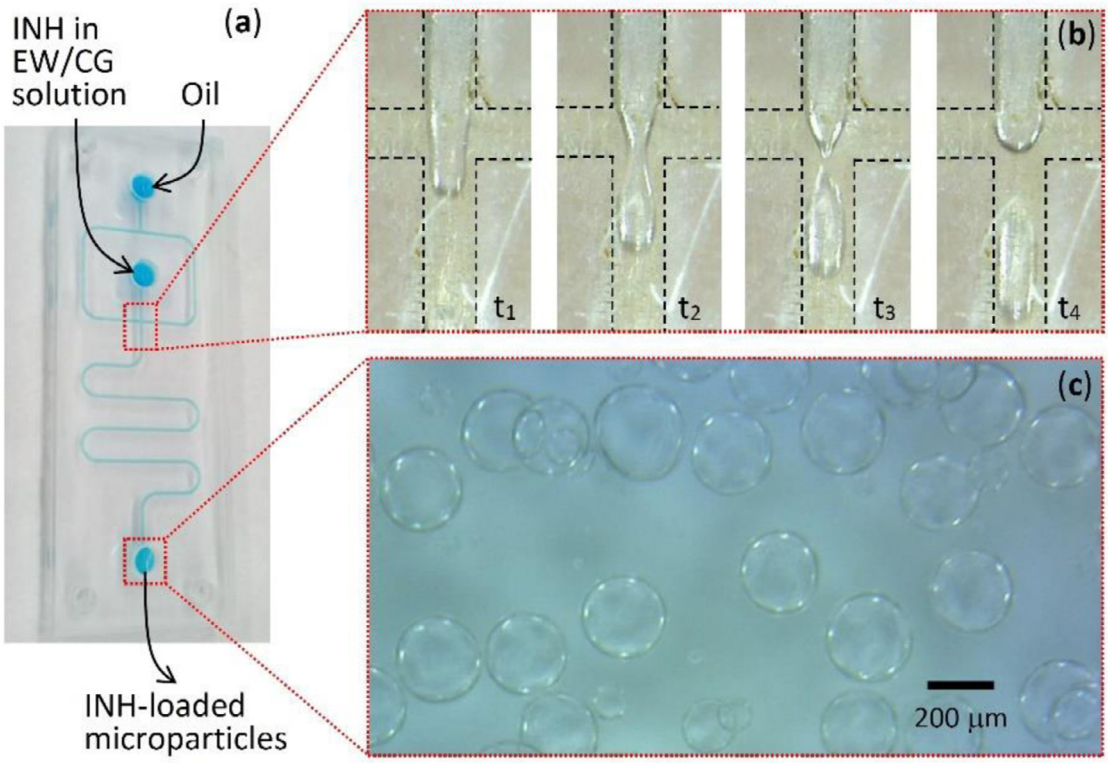

Fig. 1. (a) Photograph of the PMMA chip filled with a light-blue die to depict the fluidic network. (b) Snapshots showing the different time steps of droplet formation at the cross-junction: t_1, filling; t_2, necking; t_3, detachment; and t_4, restarting the cycle. Pictures are presented as taken, with no image editing other than cropping at the borders; the dashed lines were included for better demarcation of the microchannel walls. (c) USB microscope image of just obtained microdroplets.

2.6. Microparticles size measurement

An optical microscope (DM750, Leica Microsystems, Heerbrugg, Suiza) with integrated digital camera ICC50W was used. The diameter of individual microparticles was measured, then the average size and standard deviation were calculated. One hundred microparticles per sample were measured to provide confident statistical values. All the experiments were made in duplicate, differences between samples were not detected, and 50 images per sample were taken to perform measurements.

2.7. IR spectroscopy

INH, κ-CG and EW were analyzed as received. Particles were conditioned previous to the IR experiments to eliminate oil and water residues. Freshly prepared particles and particles from release experiments were gently twice washed with methylene chloride and allowed to dry (ambient temperature). Subsequently, the material was frozen at −80 °C and freeze-dried for 24 h at 0.014 mbar pressure in a laboratory freeze dryer (Cryodos 80, Telstar). 1–2 mg of sample was mixed with potassium bromide (100 mg) and compressed to obtain discs. IR spectrums were recorded on a FTIR-8001 PC Shimadzu spectrophotometer in the wavenumber range of 4000–400 cm^{-1} (spectral resolution: 4 cm^{-1}, number of scans: 40).

2.8. In vitro *INH release under simulated gastrointestinal conditions*

Firstly, it is worth mentioning that the primary objective of this experiment was to study the pH effect on INH release; thus, two solutions that, respectively mimic stomach and ileum pH conditions were selected, among those normally used for *in vitro* studies of TB drugs (Khatak et al., 2020; Tabriz et al., 2021). Freshly prepared particles were collected into vials. The oil phase was carefully removed using a micropipette (the oil volume to be extracted is known beforehand from the microfluidics elaboration process). Then 5.0 mL of release medium was added (NaCl 0.05 mol/L, pH 1.6). The vials were maintained at 37 °C in an orbital shaker at 150 rpm. At preselected times, aliquots (0.5 mL) were withdrawn and assayed by HPLC. An equal volume of fresh medium was added to maintain the aqueous phase constant. After 2 h, the whole volume of saline solution was gently removed and replaced by the same amount (5.0 mL) of Tris–HCl (0.1 mol/L, pH 7). The sampling procedure continued up to 24 h. The experiments were made in duplicate. INH concentration was determined by HPLC with UV detection by diode array (Prominence Series 20A, Shimadzu). The conditions of analysis were: C18 column (Zorbax Eclipse XDB, 250 × 4.6 mm, 5 μm pore size, Agilent), oven temperature 30 °C, mobile phase 35% 0.01 M KH_2PO_4 solution pH 7.0: 45% methanol: 20% acetonitrile, flow rate 1 mL/min, wavelength of detection 254 nm and injection volume 20 μL (Sankar, Sharda & Singh, 2003). A stock solution (300 mg/L) of INH in ultrapure water was prepared. Five concentration levels of standard solutions were prepared (0.5–50 mg/L) and analysed in triplicate to verify range and linearity of the analytical procedure. The calibration curve (area under the peak as a function of INH concentration) was fitted to a straight line using linear regression analysis. The evaluation of the method performance showed that the model explains ~ 99.95% (R^2) of the variation in the response variable. The corresponding correlation coefficient was $R = 0.9998$ and the p-value of the model ($p < 0.05$) indicated a significant relationship between the peak area and INH concentration.

3. Results and discussion

3.1. Microparticles shape and size

Fig. 1 shows USB microscopy images of droplets formation at the cross-junction (Fig. 1b) and generated droplets at the outlet port

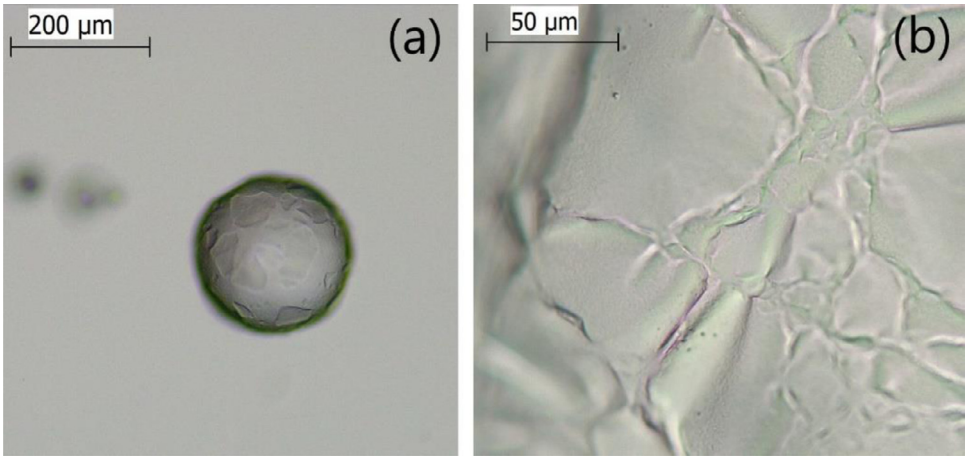

Fig. 2. Optical microcopy characterization of microparticles at different magnifications. (a) Single microparticle observed at 10X. (b) Topology of the microparticle surface observed at 40X.

(Fig. 1c) of the microfluidic device. The total flow rate was 4 mL/h and the flow rate ratio (oil to aqueous phase) was 7. In this fluid dynamic regime, the production rate was about 2 droplets per second. The regime was selected after exploring droplet generation in a wide range of operating conditions (Marengo et al., 2019). Droplet formation is governed by hydrodynamic forces that deform the jet and surface tension forces that minimize the interfacial area. At the cross-junction, the developing droplet is squeezed while gains further material, forms a thinning neck, and finally detaches downstream the junction (Fig. 1b). Droplets get perfectly spherical when they are not confined in the microchannels, as observed at the chip outlet (Fig. 1c).

Fig. 2a presents an optical microscopy image of a single microparticle. The particle surface displays different texture domains, as resulting from the complexation of proteins and polysaccharides. A more detailed picture of the microstructure is shown in Fig. 2b, where areas with different roughness are clearly distinguished. At the selected pH condition, the weak electrostatic interactions between EW proteins and CG leads to the formation of soluble complexes (Marengo et al., 2019). The MW irradiation enhances the complexation, since globular proteins denature and expose the functional groups of the amino acids (hidden into the core of the native conformation) to form covalent crosslinks (Cortés-Morales, Mendez-Montealvo & Velazquez, 2021). INH molecules are uniformly dispersed in the matrix, where the electrostatic interactions between proteins and polysaccharides stabilize the encapsulation, eventually enabling a sustained delivery under appropriate external conditions. It is worth to remark here that INH molecules are expected to be uniformly dispersed in the matrix because they are previously dissolved in the polymeric solution used to elaborate the INH-loaded microparticles (Section 2.3). Then, in the microfluidic process, microdroplets are formed from this precursor solution and subsequently cured to form microparticles.

Fig. 3 shows optical images and size distribution plots of the obtained particles. In all cases, untreated (Fig. 3a), cured at 270 W (Fig. 3c) and cured at 900 W (Fig. 3e), particles were spherical in shape and highly monodisperse. The size distribution histograms (Fig. 3b, d, and f) revealed that MW treatment did not affect the particles macrostructure, since similar average diameters were measured in all cases. In fact, MW irradiation results an excellent alternative to induce crosslinking in the biopolymer mixture, thus avoiding the addition of chemicals that could interfere with the active compound.

3.2. Particle microstructure

IR spectroscopy measurements were performed to gain knowledge on the interactions between the molecular components forming the microparticles. Fig. 4a shows the typical spectra of the individual compounds: EW, CG, and INH. For EW, the peaks at 3296, 3076 and 2935 cm^{-1} were due to the CH and NH stretching of Amide A and B. The peaks at 1655 and 1541 cm^{-1} corresponded to Amide I (C = O stretching) and Amide II (NH bending, CN stretching), respectively. In the region between 1450 and 1240 cm^{-1}, the peaks (1450, 1396, 1313 and 1240 cm^{-1}) of the Amide III (NH bending, CN stretching) were observed (Thiyagarajan et al., 2018). Fig. 4a also displays the spectrum of CG. The peaks at 3445 and 2910 cm^{-1} were due to the OH and CH stretching and the peak at 1647 cm^{-1} corresponded to polymer bonded water. The sulfate ester group signals (SO, $O = S = O$, COS) were noted at 1456, 1375, 1265, 847 and 704 cm^{-1}. The peak at 1070 cm^{-1} corresponded to the glycosidic bond and that at 927 cm^{-1} to the ether group in 3,6-anhydrogalactose (Sen & Erboz, 2010). Finally, the spectrum of INH also agreed with previously reported results (Diniz et al., 2018). NH stretching and NH bending associated to the primary and secondary amines were observed in the regions 3447–3017 cm^{-1} and 1600–1550 cm^{-1}, respectively. The peak at 1666 cm^{-1} was due to the carbonyl group of the amide and that at 1337 cm^{-1} corresponded to the CN stretching of the pyridine ring.

Fig. 4b shows the spectra of untreated particles, MW irradiated particles at 270 for 15 s, and 900 W for 15 s. Signals from INH could not be identified. This result can be explained taking into consideration the size and the mass ratio of the formulation components. Regarding the size, the molecules of the polymer and the protein are much larger than that of the antibiotic. Furthermore, the amount of EW and CG is greater than the amount of INH. Nevertheless, the three spectra appear to be quite similar, and only small differences between them can be observed. In comparison with EW and CG (Fig. 4a), the spectra of the mixture presented three noticeable peaks at 2926, 2854 and 1746 cm^{-1} which cannot be attributed neither to the protein nor to the polymer. Probably, these changes are due to the formation of carrageenan esters (C = O, 1746 cm^{-1}) or the occurrence of Maillard reaction between the carbonyl group in the galactose of these esters and amino acids of EW (Mao, Pan, Hou, Yuan & Gao, 2018). The intensity of the three peaks increased from samples corresponding to untreated particles to samples corresponding to particles irradiated at 900 W (*i.e.* at 2926 cm^{-1}, from 25.6% to 38.9%). Other minor changes were observed in the region between 1460 and 1080 cm^{-1}; for example, the peaks moved to lower wavenumbers (1095 cm^{-1} in untreated particles shifted to 1084 cm^{-1} in particles irradiated at 900 W). Finally, the interactions among the molecules can be attributed to esters formation, Maillard reaction, hydrogen bonds creation, or a combination of these mechanisms.

3.3. Kinetics of INH release

Fig. 5 shows the assay results of INH release from EW/CG microparticles. Similar release profiles were observed at both curing conditions; however, particles treated at 900 W released the INH to a lesser extent from the beginning of the assay. Burst release was not observed in either experience. During the first two hours at pH 1.6, releases of ~35% and

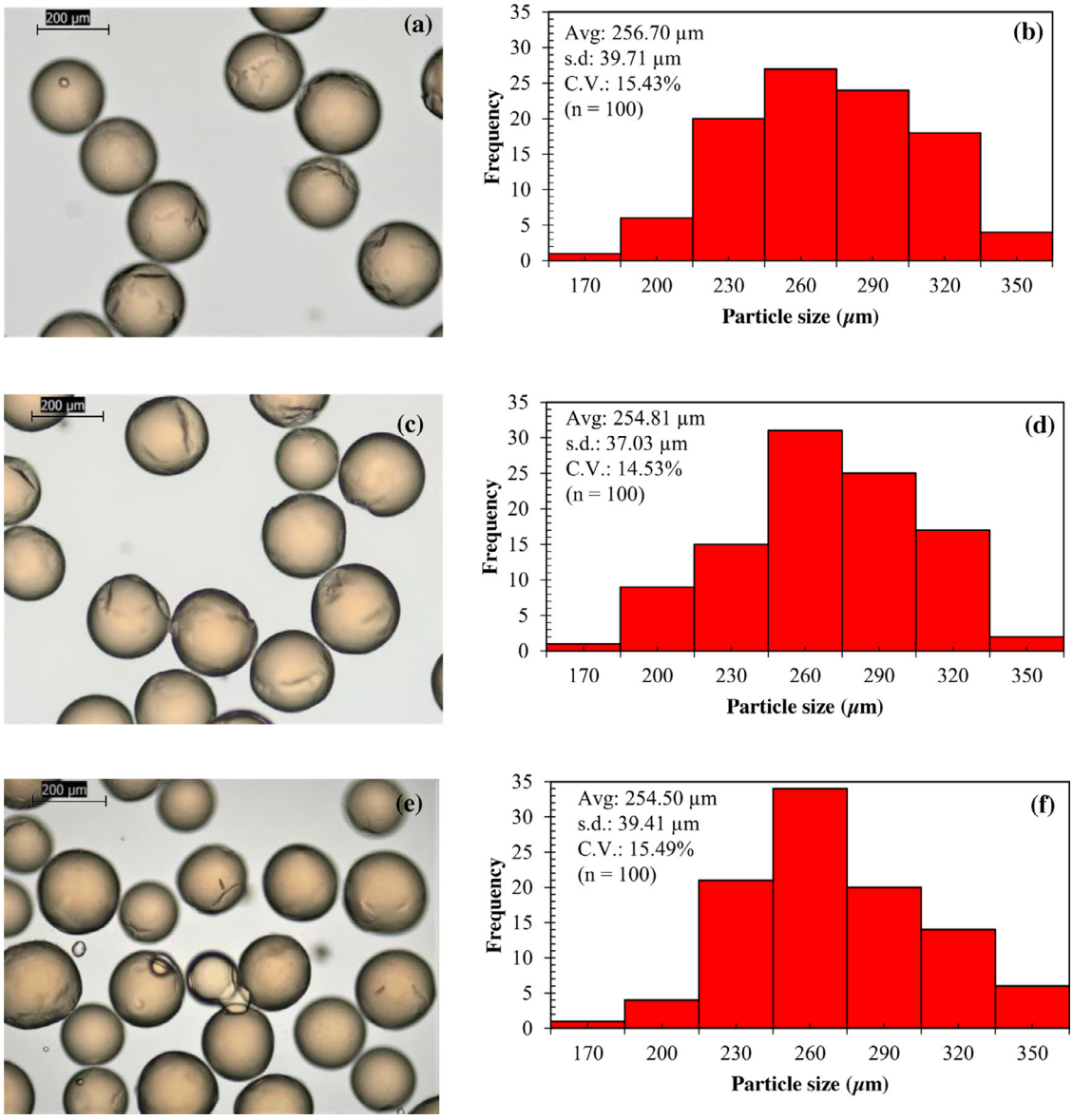

Fig. 3. Optical microscopy images at 10X magnification: (a) freshly obtained particles, (c) particles crosslinked by MW radiation at 270 W for 15 s, and (e) at 900 W for 15 s. Size distribution histograms (b), (d), and (f) correspond to the particles featured in (a), (c), and (e), respectively.

~22% were observed from particles treated at 270 and 900 W, respectively. It is evident that, as the power of irradiation increases, protein denaturation and crosslinking increases and the rate of release decreases. These are satisfactory results, because INH was poorly released under the conditions and residence time representative of the gastric tract. When the buffer was replaced (pH 7), a sudden shift of the curve slopes took place, and then the release profiles followed similar trends (Fig. 5). After 24 h, both systems showed a maximum release plateau. Particles treated at 270 W released about 83% of the drug, while particles treated at 900 W released about 65%. Thus, the proposed curing method allows one to design prototypes with adjustable delivery rates, in the pursue of optimal INH delivery systems.

In order to gain insight on the release mechanism of INH from EW/CG microparticles, data from the first 6.5 h of the *in vitro* assay were studied by using the following kinetic models (Gouda, Baishya & Qing, 2017; Higuchi, 1963; Korsmqer, Gumy, Doelker, Buri & Peppas, 1983; Wu, Bala, Skalko-Basnet & di Cagno, 2019):

$$\ln\left(Q_0 - Q\right) = \ln Q_0 - k_1 t \quad (1)$$

$$Q/Q_0 = k_H t^{1/2} \quad (2)$$

$$Q/Q_0 = k_P t^n \quad (3)$$

In all cases, Q/Q_0 represents the cumulative fraction of INH released at the time t, and k_i are the respective kinetic constants. In particular, Eq. (1) represents the first-order model, Eq. (2) is Higuchi model, and Eq. (3) is the Korsmeyer-Peppas model. The last one is commonly used to describe drug release from a polymeric matrix, where the diffusional exponent (n) characterizes the release mechanism (Korsmqer et al., 1983). The curve fittings from Eq. (3) are illustrated in the inset of Fig. 5. The values of the fitted parameters are reported in Table 1, where the mean absolute percentage deviation (ε) was included to determine the goodness of each kinetic model.

The Higuchi model presented the greatest ε values. Since this model conceives a purely diffusive process (squared root of time), the result indicates that our system would involve an additional release mechanism. Also, ε values for Eq. (2) are larger at pH 1.6 than at pH 7, indicating that the additional mechanism plays a major role at the lowest pH. On the other hand, the lowest ε values in Table 1 were obtained with the first-order model, where the release rate is directly proportional to the concentration of the remaining drug in the particle. Considering k_1, one

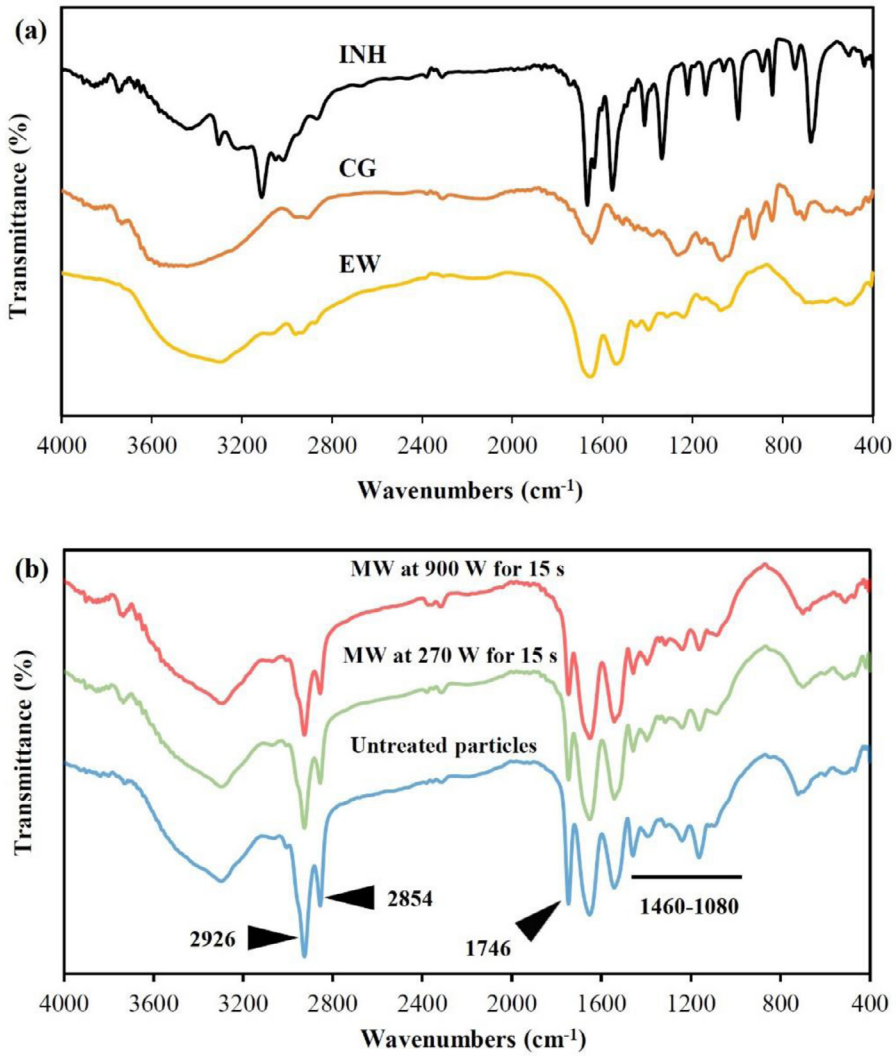

Fig. 4. FTIR spectra of: (a) individual EW, CG, and INH; (b) EW/CG/INH microparticles under different curing treatments.

Table 1
Average values and standard deviation of first-order (Eq. (1)), Higuchi (Eq. (2)), and Korsmeyer-Peppas (Eq. (3)) model parameters, and mean absolute percentage deviation (ε).

MW (W)	pH	First order k_1 (h^{-1})	ε (%)	Higuchi k_H ($h^{-0.5}$)	ε (%)	Korsmeyer-Peppas k_P (h^{-n})	n (-)	ε (%)
270	1.6	0.25±0.07	0.014	0.23±0.06	3.6	0.24±0.06	0.70±0.01	1.3
	7	0.18±0.01	0.082	0.27±0.01	0.35	0.32±0.11	0.39±0.24	0.05
900	1.6	0.13±0.01	0.001	0.12±0.01	2.9	0.13±0.01	0.72±0.13	0.12
	7	0.11± 0.04	0.024	0.18±0.05	0.44	0.20±0.02	0.44±0.26	0.09

observes that the release rate of particles treated at 900 W resulted 52% and 61% lower than those treated at 270 W, at pH 1.6 and pH 7, respectively. This information is useful to optimize the release profiles by controlling the curing conditions.

In the Korsmeyer-Peppas model, k_P provides information on the structural characteristics of microparticles. The resulting k_P values in Table 1 indicate that the release was faster at pH 7 than at pH 1.6 under both curing conditions, and that the particles cured at 270 W delivered the INH faster than the particles cured at 900 W. Also in this model, the exponent n is related to the drug release mechanism: $n < 0.5$ indicates that drug release is controlled by Fickian process, since the rate of diffusion is much smaller than the rate of microparticle wall relaxation, and $0.5 < n < 1$ (non-Fickian diffusion) occurs when the drug release is controlled by both diffusion and wall relaxation (Korsmqer et al., 1983; Langer & Peppas, 1981). Therefore, the n values reported in Table 1 suggest that the INH release followed a non-Fickian diffusion at pH 1.6, and then a Fickian diffusion at pH 7. These results agree with the fact that Higuchi model ($n = 0.5$) departs from the experimental trends at the lowest pH.

4. Conclusions

We have investigated the microfluidics-based encapsulation of INH in EW/CG microparticles and the drug delivery profiles in simulated gastrointestinal conditions. Spherical, monodisperse, and highly stable microparticles were obtained, which encapsulated the entire amount of INH loaded in the formulation. The highly hydrophilic drug remained in the particles until they were exposed to the release buffer. Different

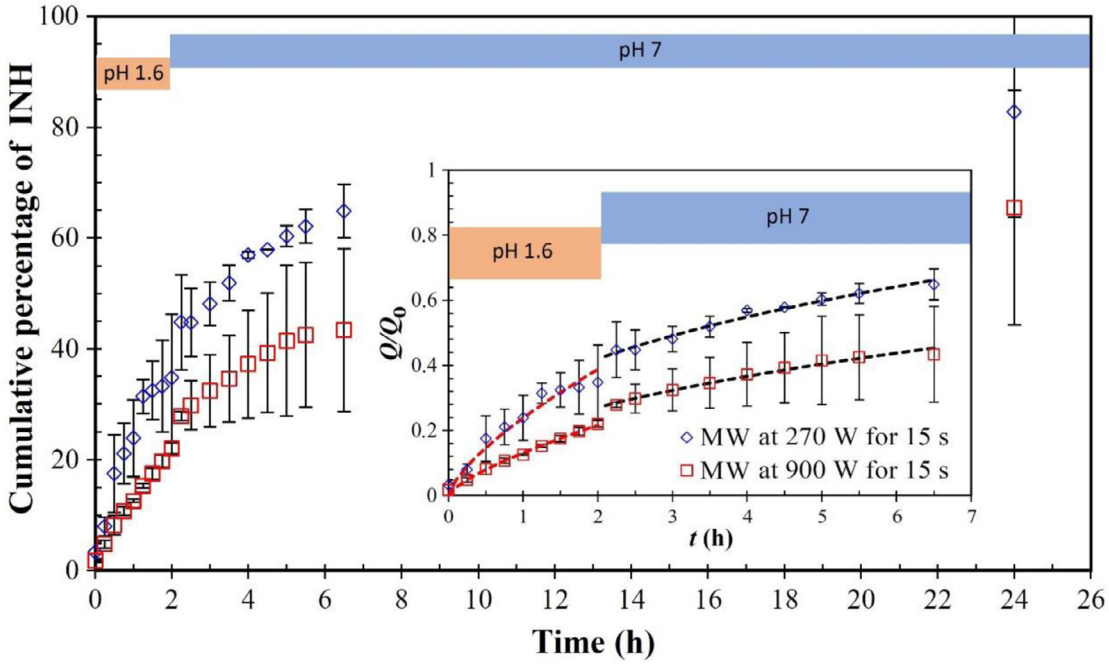

Fig. 5. *In vitro* release assay: Cumulative percentage of INH delivered by the EW/CG microparticles at 37 °C in buffer NaCl 0.05 mol/L, pH 1.6 (first 2 h) and buffer Tris–HCl 0.1 mol/L, pH 7 (the next 22 h). The inset shows an example of the fitting procedure used to obtain the kinetic model parameters. Symbols are experimental data (first 6.5 h of the experiment) and lines represent the fitting curves of Eq. (3), with parameter values reported in Table 1.

power levels of MW irradiation allowed us to modify the release profiles. The overall result of the *in vitro* assay is that particles irradiated to 900 W better approach the requisites posed in Section 1 for the formulation of INH, because only 22% of the drug was released under the gastric environment, and the remaining drug was progressively delivered in the ileum environment. Of course, *in vivo* assays would be required to gather more accurate information and feedback the formulation.

Furthermore, the release profiles were analyzed by using classical kinetic models, which enabled to hypothesize the release mechanism of INH from the protein/polysaccharide microparticles. This analysis suggests that drug delivery was faster at pH 7 than at pH 1.6, under both curing conditions, and that microparticles cured at 270 W delivered faster than those cured at 900 W. INH release followed a non-Fickian diffusion at pH 1.6, and then a Fickian diffusion at pH 7. Some degree of swelling and wall relaxation probably took place when microparticles came into contact with the release buffer at pH 1.6. Regarding kinetic equations, the best description of release profiles was given by the first-order model, according to the mean absolute percentage deviation. This knowledge, together with the information on molecular interactions in the encapsulating matrix revealed by IR spectrometry, opens further possibilities for the design of sustained release systems with desired properties. Next step in our research line is the compartmentalized loading of RIF in the same pharmaceutical prototype. Finally, it is worth to remark that these possibilities are enabled by the versatility of the microfluidic process to control the operating conditions.

Declaration of Competing Interest

The authors declare that they have no known competing financial interests or personal relationships that could have appeared to influence the work reported in this paper.

Acknowledgments

This research was conducted with the financial support from the Agencia Nacional de Promoción Científica y Tecnológica (Grants PICT 2019–03697 and PICT 2016–0228), Argentina.

References

Bale, S., Khurana, A., Reddy, A. S. S., Singh, M., & Godugu, C. (2016). Overview on therapeutic applications of microparticulate drug delivery systems. *Critical Reviews in Therapeutic Drug Carrier Systems, 33*, 309–361. 10.1615/CritRevTherDrugCarrierSyst.2016015798.

Bamshad, A., Nikfarjam, A., & Khaleghi, H. (2016). A new simple and fast thermally-solvent assisted method to bond PMMA–PMMA in microfluidics devices. *Journal of Micromechanics and Microengineering, 26*, Article 065017 (12pp). 10.1088/0960-1317/26/6/065017.

Barberis, I., Bragazzi, N. L., Galluzzo, L., & Martini, M. (2017). The history of tuberculosis: From the first historical records to the isolation of Koch's bacillus. *J. Prev. Med. Hyg., 58*, E9–E12. 10.15167/2421-4248/JPMH2017.58.1.728.

Booysen, L. L. I. J., Kalombo, L., Brooks, E., Hansen, R., Gilliland, J., Gruppo, V., … du Plessis, L. H. (2013). *In vivo/in vitro* pharmacokinetic and pharmacodynamic study of spray-dried poly-(dl-lactic-co-glycolic) acid nanoparticles encapsulating rifampicin and isoniazid. *International Journal of Pharmaceutics, 444*, 10–17. 10.1016/j.ijpharm.2013.01.038.

Choi, A., Seo, K. D., Kim, D. W., Kim, B. C., & Kim, D. S. (2017). Recent advances in engineering microparticles and their nascent utilization in biomedical delivery and diagnostic applications. *Lab on a chip, 17*, 591–613. 10.1039/c6lc01023g.

Cortés-Morales, E. A., Mendez-Montealvo, G., & Velazquez, G. (2021). Interactions of the molecular assembly of polysaccharide-protein systems as encapsulation materials. A review. *Advances in Colloid and Interface Science, 295*, Article 102398. 10.1016/j.cis.2021.102398.

Diniz, L. F., Souza, M. S., Carvalho, P. S., da Silva, C. C. P., D'Vries, R. F., & Ellena, J. (2018). Novel isoniazid cocrystals with aromatic carboxylic acids: Crystal engineering, spectroscopy and thermochemical investigations. *Journal of Molecular Structure, 1153*, 58–68. 10.1016/j.molstruc.2017.09.115.

Ghanizadeh Tabriz, A., Nandi, U., Hurt, A. P., Hui, H. W., Karki, S., Gong, Y., et al. (2021). 3D printed bilayer tablet with dual controlled drug release for tuberculosis treatment. *International Journal of Pharmaceutics, 593*, Article 120147. 10.1016/j.ijpharm.2020.120147.

Gouda, R., Baishya, H., & Qing, Z. (2017). Application of mathematical models in drug release kinetics of carbidopa and levodopa ER tablets. *Journal of Developing Drugs, 6*, Article 1000171. 10.4172/2329-6631.1000171.

Grenha, A., Alves, A. D., Guerreiro, F., Pinhoc, J., Simões, S., Almeida, A. J., et al. (2020). Inhalable locust bean gum microparticles co-associating isoniazid and rifabutin: Therapeutic assessment in a murine model of tuberculosis infection. *European Journal of Pharmaceutics and Biopharmaceutics, 147*, 38–44. 10.1016/j.ejpb.2019.11.009.

Gürsoy, A., Kut, E., & Özkırımlı, S. (2004). Co-encapsulation of isoniazid and rifampicin in liposomes and characterization of liposomes by derivative spectroscopy. *International Journal of Pharmaceutics, 271*, 115–123. 10.1016/j.ijpharm.2003.10.033.

(2008). Handbook of anti-tuberculosis agents. *Tuberculosis, 88*(2), 85–86. 10.1016/S1472-9792(08)70002-7.

Higuchi, T. (1963). Mechanism of sustained- action medication theoretical analysis of rate

of release of solid drugs dispersed in solid matrices. *Journal of Pharmaceutical Sciences, 52*, 1145–1149. 10.1002/jps.2600521210.

Hong, T. F., Ju, W. J., Wu, M. C., Tai, C. H., Tsai, C. H., & Fu, L. M. (2010). Rapid prototyping of PMMA microfluidic chips utilizing a CO_2 laser. *Microfluidics and Nanofluidics, 6*, 1125–1133. 10.1007/s10404-010-0633-0.

Khatak, S., Mehta, M., Awasthi, R., Paudel, K. R., Singh, S. K., Gulati, M., et al. (2020). Solid lipid nanoparticles containing anti-tubercular drugs attenuate the Mycobacterium marinum infection. *Tuberculosis, 125*, Article 102008. 10.1016/j.tube.2020.102008.

Kim, J. H., Jeon, T. Y., Choi, T. M., Shim, T. S., Kim, S. H., & Yang, S. M. (2014). Droplet microfluidics for producing functional microparticles. *Langmuir: the ACS Journal of Surfaces and Colloids, 30*, 1473. 10.1021/la403220p.

Kong, T., Wu, J., To, M., Yeung, K., Shum, H., & Wang, L. (2012). Droplet based microfluidic fabrication of designer microparticles for encapsulation applications. *Biomicrofluidics, 6*, Article 034104. 10.1063/1.4738586.

Korsmqer, R. W., Gumy, R., Doelker, E., Buri, P., & Peppas, N. A. (1983). Mechanisms of solute release from porous hydrophilic polymers. *International Journal of Pharmaceutics, 15*, 25–35. 10.1016/0378-5173(83)90064-9.

Langer, R. S., & Peppas, N. A. (1981). Present and future applications of biomaterials in controlled drug delivery systems. *Biomaterials, 2*, 201–214. 10.1016/0142-9612(81)90059-4.

Liga, A., Morton, J. A. S., & Kersaudy-Kerhoas, M. (2016). Safe and cost-effective rapid-prototyping of multilayer PMMA microfluidic devices. *Microfluidics and Nanofluidics, 20*, 164. 10.1007/s10404-016-1823-1.

Liu, K., Xiang, J., Ai, Z., Zhang, S., Fang, Y., Chen, T., et al. (2017). PMMA microfluidic chip fabrication using laser ablation and low temperature bonding with OCA film and LOCA. *Microsystem Technologies, 23*, 1937–1942. 10.1007/s00542-016-2924-1.

Mao, L., Pan, Q., Hou, Z., Yuan, F., & Gao, Y. (2018). Development of soy protein isolate-carrageenan conjugates through maillard reaction for the microencapsulation of *Bifidobacterium longum*. *Food Hydrocolloids, 84*, 489–497. 10.1016/j.foodhyd.2018.06.037.

Marengo, R. C., Olivares, M. L., & Berli, C. L. A. (2019). Generation of egg white/carrageenan microparticles by droplet-based microfluidics. *Journal of Food Engineering, 259*, 21–28. 10.1016/j.jfoodeng.2019.04.019.

Mukhtar, M., Pallagi, E., Csóka, I., Benke, E., Farkas, Á., Zeeshan, M., et al. (2020). Aerodynamic properties and *in silico* deposition of isoniazid loaded chitosan/thiolated chitosan and hyaluronic acid hybrid nanoplex DPIs as a potential TB treatment. *International Journal of Biological Macromolecules, 165*, 3007–3019. 10.1016/j.ijbiomac.2020.10.192.

Mwila, C., & Walker, R. B. (2020). Improved stability of rifampicin in the presence of gastric-resistant isoniazid microspheres in acidic media. *Pharmaceutics, 12*, 234. 10.3390/pharmaceutics12030234.

Nkanga, C. I., Krause, R. W., Noundou, X. S., & Walker, R. B. (2017). Preparation and characterization of isoniazid-loaded crude soybean lecithin liposomes. *International Journal of Pharmaceutics, 526*, 466–473. 10.1016/j.ijpharm.2017.04.074.

Pandey, G., Yadav, S. K., & Mishra, B. (2015). Preparation and characterization of isoniazid and lamivudine co-loaded polymeric microspheres. *Artificial Cells, Nanomedicine, and Biotechnology, 44*(8), 1867–1877. 10.3109/21691401.2015.1111229.

Rani, S., Gothwal, A., Khan, I., Pachouri, P. K., Bhaskar, N., Gupta, U. D., et al. (2018). Smartly engineered PEGylated Di-Block nanopolymeric micelles: Duo delivery of isoniazid and rifampicin against mycobacterium tuberculosis. *AAPS PharmSciTech, 19*, 3237–3248. 10.1208/s12249-018-1151-8.

Rodrigues, S., Cunha, L., Rico, J., Rosa da Costa, A. M., Almeida, A. J., Faleiro, M. L., et al. (2020). Carrageenan from red algae: An application in the development of inhalable tuberculosis therapy targeting the macrophages. *Drug Delivery and Translational Research, 10*, 1675–1687. 10.1007/s13346-020-00799-0.

Sankar, R., Sharda, N., & Singh, S. (2003). Behavior of decomposition of rifampicin in the presence of isoniazid in the pH range 1-3. *Drug Development and Industrial Pharmacy, 29*, 733–738. 10.1081/DDC-120021772.

Sen, M., & Erboz, E. N. (2010). Determination of critical gelation conditions of κ-carrageenan by viscosimetric and FT-IR analyses. *Food Research International, 43*, 1361–1364 (Ottawa, Ont.). 10.1016/j.foodres.2010.03.021.

Sheth, U., Tiwari, S., & Bahadur, A. (2018). Preparation and characterization of anti-tubercular drugs encapsulated in polymer micelles. *Journal of Drug Delivery Science and Technology, 48*, 422–428. 10.1016/j.jddst.2018.10.021.

Shrimal, P., Jadeja, G., & Patel, S. (2020). A review on novel methodologies for drug nanoparticle preparation: Microfluidic approach. *Chemical Engineering Research and Design, 153*, 728–756. 10.1016/j.cherd.2019.11.031.

Singh, H., Bhandari, R., & Kaur, I. P. (2013). Encapsulation of rifampicin in a solid lipid nanoparticulate system to limit its degradation and interaction with isoniazid at acidic pH. *International Journal of Pharmaceutics, 446*, 106–111. 10.1016/j.ijpharm.2013.02.012.

Singh, S., Mariappan, T. T., Sankar, R., Sarda, N., & Singh, B. (2001). A critical review of the probable reasons for the poor/variable bioavailability of rifampicin from anti-tubercular fixed-dose combination (FDC) products, and the likely solutions to the problem. *International Journal of Pharmaceutics, 228*, 5–17. 10.1016/S0378-5173(01)00754-2.

Tabriz, A. G., Nandi, U., Hurt, A. P., Hui, H. W., Karki, S., Gong, Y., et al. (2021). 3D printed bilayer tablet with dual controlled drug release for tuberculosis treatment. *International Journal of Pharmaceutics, 593*, Article 120147. 10.1016/j.ijpharm.2020.120147.

Thiyagarajan, A., Bharti, V. K., Tyagi, S., Tyagi, P. K., Ahuja, A., Kumar, K., et al. (2018). Synthesis of non-toxic, biocompatible, and colloidal stable silver nanoparticle using egg-white protein as capping and reducing agents for sustainable antibacterial application. *RSC Advances, 8*, 23213–23229. 10.1039/c8ra03649g.

Wu, I. Y., Bala, S., Skalko-Basnet, N., & di Cagno, M. P. (2019). Interpreting non-linear drug diffusion data: Utilizing korsmeyer-peppas model to study drug release from liposomes. *European Journal of Pharmaceutical Sciences, 138*, Article 105026. 10.1016/j.ejps.2019.105026.

Wu, J., Kong, T., Yeung, K., Shum, H., Cheung, K., Wang, L., et al. (2013). Fabrication and characterization of monodisperse PLGA–alginate core–shell microspheres with monodisperse size and homogeneous shells for controlled drug release. *Acta biomaterialia, 9*, 7410–7419. 10.1016/j.actbio.2013.03.022.